Pressure-volume equation of state of the high-pressure $B2$ phase of NaCl

Nagayoshi Sata,* Guoyin Shen, Mark L. Rivers,† and Stephen R. Sutton†
Consortium for Advanced Radiation Sources, University of Chicago, Argonne, Illinois 60439
(Received 4 July 2001; published 4 March 2002)

We have measured the unit-cell volume of the high-pressure $B2$ phase of NaCl up to 68 GPa in a diamond anvil cell with the laser annealing technique and synchrotron radiation. Laser annealing promotes the release of nonhydrostatic stress in the sample chamber, resulting in a quasihydrostatic condition for the sample at high pressures and an associated precision increase in the unit-cell volume determination. Since the $B2$ phase is only stable over 30 GPa, it is difficult to use the conventional Birch-Murnaghan equation of state (EOS) due to the lack of volume information at zero pressure. We adopted a modified data treatment which uses a reference volume V_r at any pressure instead of the zero-pressure volume V_0. The modified third-order Birch-Murnaghan EOS is expressed by the pressure (P_r), bulk modulus (K_r), and pressure dependence of the bulk modulus (K_r') at the reference point. We also fitted our data to the modified universal EOS, with which infinite zero-pressure volume can be treated. All these treatments yield reasonably consistent results. We calculated the pressure dependence of the bulk modulus and compared the result with other materials generally used as pressure media. The bulk modulus of the $B2$ phase of NaCl is similar to that of the $B1$ phase around the transition pressure, but it increases faster with pressure. The bulk modulus data show that, at $P=100$ GPa, the $B2$ phase of NaCl ($K\sim420$ GPa) is harder than argon ($K\sim360$ GPa), but still softer than MgO ($K\sim500$ GPa).

DOI: 10.1103/PhysRevB.65.104114 PACS number(s): 64.30.+t, 64.10.+h

I. INTRODUCTION

NaCl is one of the simplest ionic crystals. The structure of NaCl transforms from rock salt structure (the $B1$ phase) into CsCl structure (the $B2$ phase) at about 30 GPa.[1–3] Understanding this pressure-induced transformation is a prerequisite for the understanding of more complex systems. The equation of state (EOS) of the NaCl-B1 phase has been well studied for its importance as one of the simplest ionic crystals and a commonly used pressure calibrant at pressures below 30 GPa.[4–6] Detailed information on the phase transition and on the NaCl-$B2$ phase would be useful in understanding this classic system and in extending the usable pressure range of the calibrant. However, such data are limited.[2,7,8] We performed high-pressure experiments to measure the volume-pressure relations of the NaCl-$B2$ phase up to 68 GPa with the use of a diamond anvil cell (DAC) and laser-heated annealing techniques. The use of the laser annealing technique dramatically reduces the nonhydrostatic stress in the sample chamber, resulting in a more precise unit-cell volume determination at high pressures and at room temperature. From these data, we calculated the pressure dependence of the bulk modulus of the $B2$ phase and estimated the change in the volume and bulk modulus at the $B1$-$B2$ transition point.

II. EXPERIMENTS AND RESULTS

A diamond anvil cell, with culet size of 300 μm, was used to generate high-pressure conditions. The rhenium gasket was preindented to 30 μm in thickness, and a hole of 120 μm was drilled as a sample chamber. We ground both MgO (99.99%, Kanto Kagaku) and NaCl (99.99%, Alfa Aesar) down to less than 10 μm and mixed fine Pt powder (99.9%, Aldrich) and MgO by a volume ratio of 1:4. Both the Pt-MgO mixture and the NaCl powder were pressed to disks with thickness less than 10 μm. Four disks of powdered samples (NaCl, two Pt+MgO mixtures, and NaCl) were placed in the sample chamber. The whole assembly was put in a vacuum oven at 120 °C for about 30 min before the pressure was applied to avoid any moisture. Our experimental procedure was as follows: increase the pressure at room temperature to a desired point, obtain x-ray diffraction patterns before and after laser annealing, increase the pressure to the next level, and repeat until the anvil failed at 68 GPa. A YLF laser heating system[9] was used for annealing. The laser heating spot size at the sample position was about 20 μm in diameter. A 45-μm-square area at the central position was scanned by the heating laser for a total time of about 3 min for each annealing. Annealing at a temperature around 1200 K helps to release the nonhydrostatic stress. No clear crystal growth was observed by keeping the temperature below 1200 K. The angle-dispersive x-ray diffraction experiments were performed at the GeoSoilEnviroCARS beamline (13-BM-D) at the Advanced Photon Source (APS). A monochromatic x-ray beam (energy 29.200 keV) was produced by a channel-cut crystal (silicon [220]). The x-ray beam was controlled by a slit system to a size of 150×150 μm^2 and consequently focused to a beam size of 7 μm (vertical) $\times10$ μm (horizontal) at a full width at half maximum (FWHM) by Kirkpatrick-Baez mirrors.[10] A charge-coupled device (CCD) detector (Bruker-2k) was used for diffraction measurements. Exposure time for the CCD was 5 min. We applied a spatial correction using a previously measured grid image. The sample-detector distance and inclination of the detector are calibrated from a standard material (CeO_2) at 1 atm. We used the FIT2D (Ref. 11) program to integrate two-dimensional (2D) patterns to produce 1D profiles. Figure 1 shows a typical integrated pattern. Strong [111] and [200] peaks of Pt (denoted $[111]_{Pt}$ and $[200]_{Pt}$), [110] peak of the

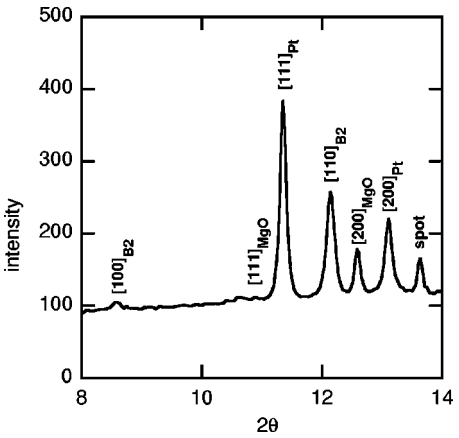

FIG. 1. This x-ray pattern (run No. 37) shows the typical peak intensities in this study. $[100]_{B2}$ represents the [100] peak of the NaCl-B2 phase, etc. The measured pressure is 68.5 (9) GPa by the lattice parameters of Pt (Ref. 12). The peak at 2θ of about 13.7° is a single spot in the diffraction image which remains unidentified. The $[100]_{B2}$ and $[111]_{MgO}$ are used only for estimating errors due to their low intensities.

$B2$ phase of NaCl ($[110]_{B2}$), and [200] peak of MgO ($[200]_{MgO}$) were observed in the diffraction patterns. Weak $[100]_{B2}$ and $[111]_{MgO}$ peaks were also observed. We used the PEAKFIT program for determining peak positions with a single Voigt function. Since $[111]_{MgO}$ is close to the [100] peak of Re, multiple peak fitting was used in this region. The peak position of $[111]_{MgO}$ may contain larger errors than other peaks because of this overlap. Pressures were obtained from lattice parameters of Pt (Ref. 12) and MgO (Ref. 13) and are denoted as P_{Pt} and P_{MgO}. The $[111]_{MgO}$ and $[100]_{B2}$ peaks were used only for estimating errors due to their low intensities. Table I summarizes all our data for *d*-spacing and pressure determinations.

III. DATA ANALYSIS

From lattice strain theory, the relative shift among different diffraction lines that results from uniaxial stress can be described as a function of the elastic anisotropy *S*, the uniaxial stress component *t*, and geometrical parameters.[14] Shim *et al.*[15] used multiplication of the elastic anisotropy and the uniaxial stress component, the St value, as an indicator of the magnitude of the uniaxial stress in a sample. Figure 2 shows our calculated St values from two Pt peaks. All St values after laser annealing are found to be smaller than 0.005, a value Shim *et al.*[15] used as the criterion of a quasihydrostatic condition. Speziale *et al.*[13] estimated the stress condition of MgO from the difference of the calculated unit-cell parameter *a* from each diffraction peak. Nonhydrostatic conditions are inferred when the normalized difference is over 0.6% between [200] and [111] peaks of MgO. When the difference is less than 0.1%, the stress condition is considered to be quasihydrostatic. Our data for MgO show that the normalized difference was less than 0.2% (Fig. 3). Therefore, data after annealing are used for establishing the equation of state.

The obtained data were fitted to two kinds of equations of state: the Birch-Murnaghan EOS (Ref. 16) and the universal EOS (Ref. 17). With the Birch-Murnaghan EOS, the pressure-volume data are recast in terms of a strain parameter $g=1/2[(V/V_{01})^{-2/3}-1]$ and a normalized stress $G=P/3(1+2g)^{-5/2}$. Here V_{01} is the normalized zero-pressure volume of the $B1$ phase: 44.86 Å^3. Heinz and Jeanloz[7] used a g-G plot to estimate the zero-pressure volume of the $B2$ phase from the cross point of the $G=0$ axis. We adopted their approach and plotted the g-G relation from our P_{Pt} and V_{B2} data with linear and second-order polynomial fits (Fig. 4). The linear and second-order polynomial function in the g-G plane correspond to the second- and third-order Birch-Murnaghan EOS, respectively. As can be seen from Fig. 4, the linear equation does not give a good fit to our data, while the use of the second-order polynomial leads to a reasonable fit. However, we cannot obtain the zero-pressure volume with the second-order polynomial, because the fit never crosses the $G=0$ axis. To avoid this problem, we modified the Birch-Murnaghan EOS by introducing a reference volume V_r instead of the zero-pressure volume V_0. The Birch-Murnaghan EOS is derived from expanding the free energy in powers of the Eulerian strain (e.g., Ref. 18) with the conditions $P,K,K' \rightarrow P_0=0,K_0,K_0'$ at $V \rightarrow V_0$ (subscripts 0 denote zero-pressure values). When the Birch-Murnaghan EOS is modified, the conditions are changed to $P,K,K' \rightarrow P_r,K_r,K_r'$ at $V \rightarrow V_r$ (subscripts r refer a reference point). The modified third-order Birch-Murnaghan EOS thus reads

$$P=\left\{P_r-\frac{1}{2}(3K_r-5P_r)\left[1-\left(\frac{V}{V_r}\right)^{-2/3}\right]+\frac{9}{8}K_r\left(K_r'-4+\frac{35P_r}{9K_r}\right)\left[1-\left(\frac{V}{V_r}\right)^{-2/3}\right]^2\right\}\left(\frac{V}{V_r}\right)^{-5/3}, \tag{1a}$$

$$K=K_r\left\{1+\frac{1}{2}(5-3K_r')\left[1-\left(\frac{V}{V_r}\right)^{-2/3}\right]+\frac{27}{8}K_r\left(K_r'-4+\frac{35P_r}{9K_r}\right)\left[1-\left(\frac{V}{V_r}\right)^{-2/3}\right]^2\right\}\left(\frac{V}{V_r}\right)^{-5/3}. \tag{1b}$$

If we fix $K_r'=4-35P_r/9K_r$, we obtain the modified second-order Birch-Murnaghan EOS. If we chose $V_r=V_0$, we obtain the original Birch-Murnaghan EOS referenced to zero pressure.

We assumed a reference volume of $V_r=27.17$ Å^3, which is the value reported by Bassett *et al.*[1] as the volume of the NaCl-B2 phase at the $B1$-$B2$ transition point. Then P_r and K_r correspond to the pressure and bulk modulus at the transition point. The fitting parameters are shown in Table II along with the calculated pressure residuals R_P between the observed data and calculated data where

$$R_P=\sqrt{\frac{\Sigma(P_{cal}-P_{obs})^2}{n}} \quad (n: \text{ number of data points}). \tag{2}$$

TABLE I. Observed data. The numbers in parentheses are uncertainties in the last digit(s).

	Pt			MgO			NaCl-B2		
No.	$d_{[111]}$ (Å)	$d_{[200]}$ (Å)	P_{Pt} [a] (GPa)	$d_{[111]}$ (Å)	$d_{[200]}$ (Å)	P_{MgO} [b] (GPa)	$d_{[100]}$ (Å)	$d_{[110]}$ (Å)	V_{B2} (Å^3)
8	2.2062(4)	1.9143(7)	25.2(17)	2.306(6)	2.0088(7)	30.3(50)	3.000(3)	2.1193(2)	26.92(9)
9[c,d]	2.19064(8)	1.89873(7)	34.9(9)	2.310(2)	1.9980(2)	34.9(12)	2.989(2)	2.1129(2)	26.68(2)
11	2.2036(3)	1.9105(2)	27.1(10)	2.3199(3)	2.0103(3)	29.7(5)	3.008(2)	2.1251(4)	27.15(7)
12[c]	2.1986(3)	1.9045(2)	30.5(3)	2.320(6)	2.0064(1)	31.3(11)	3.0111(9)	2.1296(3)	27.32(2)
13[c]	2.1948(3)	1.9019(3)	32.5(6)	2.313(2)	2.0015(2)	33.4(9)	3.001(2)	2.1176(4)	26.86(2)
14[c]	2.1902(2)	1.8975(2)	35.5(4)	2.307(2)	1.9953(2)	36.1(10)	2.9851(9)	2.1070(2)	26.46(2)
16[c]	2.1867(3)	1.8946(3)	37.7(5)	2.304(2)	1.9899(2)	38.5(24)	2.9670(5)	2.0981(5)	26.12(1)
17[c]	2.1807(3)	1.8894(2)	41.6(5)	2.300(2)	1.9813(2)	42.5(33)	2.9485(7)	2.0820(3)	25.53(2)
18	2.1779(4)	1.8879(4)	43.1(10)	2.281(5)	1.9782(2)	44.0(13)	2.9369(8)	2.0761(3)	25.31(3)
19[c]	2.1737(4)	1.8844(3)	46.0(12)	2.278(11)	1.9721(9)	47.0(3)	2.923(2)	2.0653(3)	24.91(7)
20	2.1721(3)	1.8833(1)	47.0(14)	2.277(4)	1.9708(2)	47.7(4)	2.921(2)	2.0620(4)	24.80(19)
21[c]	2.1689(3)	1.8796(2)	49.6(8)	2.2714(5)	1.9657(2)	50.3(8)	2.910(3)	2.0538(4)	24.50(15)
22	2.1684(2)	1.8795(3)	49.8(10)	2.272(4)	1.9648(2)	50.8(14)	2.908(2)	2.0532(4)	24.48(10)
23[c]	2.1661(3)	1.8769(3)	51.8(7)	2.265(6)	1.9624(4)	52.1(5)	2.898(2)	2.0476(4)	24.28(6)
24	2.1651(2)	1.8761(2)	52.5(7)	2.265(2)	1.9604(2)	53.2(6)	2.899(2)	2.0444(2)	24.17(19)
25[c]	2.1616(3)	1.8730(4)	55.1(7)	2.259(3)	1.9560(3)	55.6(1)	2.888(2)	2.0366(3)	23.89(20)
26	2.1611(2)	1.8729(4)	55.4(9)	2.258(3)	1.9549(4)	56.2(5)	2.881(2)	2.0364(4)	23.89(4)
27[c]	2.1586(4)	1.8702(3)	57.6(6)	2.258(3)	1.9523(2)	57.6(17)	2.878(2)	2.0320(3)	23.73(11)
28	2.1573(4)	1.8696(3)	58.3(9)	2.255(4)	1.9508(2)	58.5(12)	2.8762(6)	2.0300(3)	23.66(14)
29[c]	2.1559(2)	1.8683(3)	59.5(9)	2.247(2)	1.9480(2)	60.1(14)	2.867(2)	2.0262(2)	23.53(6)
30	2.1554(2)	1.8680(3)	59.9(9)	2.252(3)	1.9477(2)	60.3(13)	2.867(3)	2.0254(2)	23.50(7)
31[c]	2.1537(3)	1.8665(2)	61.2(10)	2.243(2)	1.9468(3)	60.8(28)	2.866(3)	2.0218(2)	23.38(18)
32	2.1522(3)	1.8652(4)	62.4(10)	2.249(3)	1.9437(2)	62.6(24)	2.848(5)	2.0184(2)	23.26(16)
33[c]	2.1508(2)	1.8637(2)	63.7(8)	2.243(2)	1.9418(4)	63.7(7)	2.856(3)	2.0161(4)	23.18(13)
34	2.1500(2)	1.8633(2)	64.2(10)	2.243(2)	1.9409(2)	64.3(12)	2.853(2)	2.0146(4)	23.13(9)
35[c]	2.1486(3)	1.8613(2)	66.0(8)	2.2408(7)	1.9391(2)	65.4(9)	2.847(2)	2.0112(2)	23.01(6)
36	2.1469(3)	1.8607(4)	66.8(10)	2.238(2)	1.9371(2)	66.6(8)	2.845(2)	2.0091(4)	22.94(9)
37[c]	2.1450(2)	1.8588(2)	68.5(9)	2.236(2)	1.9352(2)	67.9(7)	2.838(4)	2.0059(4)	22.83(3)
38	2.1447(2)	1.8587(2)	68.7(10)	2.2376(2)	1.9342(1)	68.5(24)	2.838(1)	2.0047(3)	22.79(8)

[a]Based on the EOS data from Holmes *et al.* (Ref. 12).

[b]Based on the EOS data from Speziale *et al.* (Ref. 13).

[c]After laser annealing.

[d]Imaging plate data, read by the Fuji BAS-2500 system at the Bio-CAT (Sector 18) at the APS.

We also used the universal EOS (Ref. 17) to fit our data. This EOS is widely accepted for highly compressible solids. Although this EOS contains the zero-pressure volume term, it is less sensitive to this parameter than the Birch-Murnaghan EOS. Our approach was to assume a zero-pressure volume V_0 and then minimize the pressure residual R_P. Figure 5 is the relation between V_0 and R_P using the data of P_{Pt} and P_{MgO}. It is shown that small residuals can be obtained from a large range of V_0 values. Therefore, with the universal EOS, V_0 is not a critical parameter in characterizing the compression behavior of the NaCl-$B2$ phase. As with the Birch-Murnaghan EOS treatment, we modified the universal EOS for the infinite zero-pressure volume by introducing a reference point. The universal EOS (Ref. 17) is derived from a scaled separation a^* and an empirical potential E: $a^*=(r_{WS}-r_{WSE})/l$ and $E=E_0(1+a^*)\exp(-a^*)$. Here l is the scaling length; r_{WS} is the average Wigner-Seitz radius and is given by $V=4\pi r_{WS}^3$, where V is the specific volume per atom. The zero-pressure value of r_{WS} is denoted by r_{WSE}. We changed the base of a^* to a different nonzero reference r_{WSR}, which is between r_{WS} and r_{WSE}. Then a^* and E were expressed by these formulas: $a^*=b^*+a_r^*$ and $E=E_r[1+b^*/(1+a_r^*)]\exp(-b^*)$. Here $b^*=(r_{WS}-r_{WSR})/l$ and $a_r^*=(r_{WSR}-r_{WSE})/l$. The value of E at the reference point is denoted E_r. The r_{WSE} increases to infinity and the a_r^* decreases to negative infinity as the zero-pressure volume V_0 increases to infinity. Then the empirical potential E for the infinite zero-pressure volume is expressed with b^* using this formula: $E=E_r\exp(-b^*)$.

Poirier[18] pointed out that the universal EOS can be obtained through the same derivation as the Birch-Murnaghan EOS, using a strain parameter $\varepsilon=(V/V_0)^{1/3}-1$ and the free energy $F=F_0(1+A\varepsilon)\exp(-A\varepsilon)$ (F_0, A: constant). For the modified universal EOS, we chose a strain parameter $\varepsilon=(V/V_r)^{1/3}-1$ and a free energy $F=F_r\exp(-A\varepsilon)$ (F_r, A:

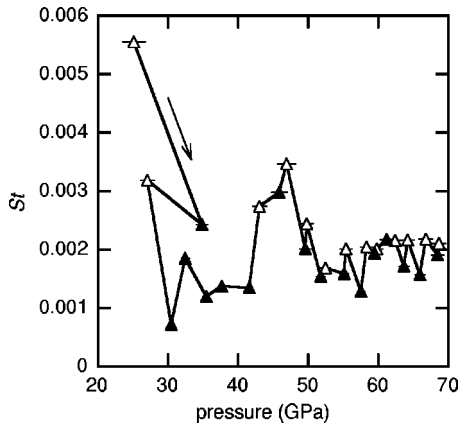

FIG. 2. The St values, the multiplication of the elastic anisotropy S, and the uniaxial stress component t, from the diffraction of Pt. These values signify the uniaxial stress conditions in the sample (Ref. 14). Solid line, experimental path; open triangle, before annealing; solid triangle, after annealing. The effect of laser annealing on these values can be seen. All values after annealing are less than 0.005, a value that Shim *et al.* (Ref. 15) takes as the criterion of the quasihydrostatic condition.

constant). We obtained the following expressions for P and K with V:

$$P = P_r\left(\frac{V}{V_r}\right)^{-2/3} \exp\left\{-\left(\frac{3K_r}{P_r}-2\right)\left[\left(\frac{V}{V_r}\right)^{1/3}-1\right]\right\}, \quad (3a)$$

$$K = \left\{K_r + \left(K_r - \frac{2P_r}{3}\right)\left[\left(\frac{V}{V_r}\right)^{1/3}-1\right]\right\}\left(\frac{V}{V_r}\right)^{-2/3} \times \exp\left\{-\left(\frac{3K_r}{P_r}-2\right)\left[\left(\frac{V}{V_r}\right)^{1/3}-1\right]\right\}. \quad (3b)$$

Here P_r and K_r is the pressure and bulk modulus at the reference point ($V=V_r$). As in the Birch-Murnaghan EOS treatment, we assumed a reference volume of $V_r = 27.17$ Å^3. Then P_r and K_r correspond to the pressure and bulk modulus at the transition point. The fitting results are shown in Table II with the pressure residual using Eq. (2).

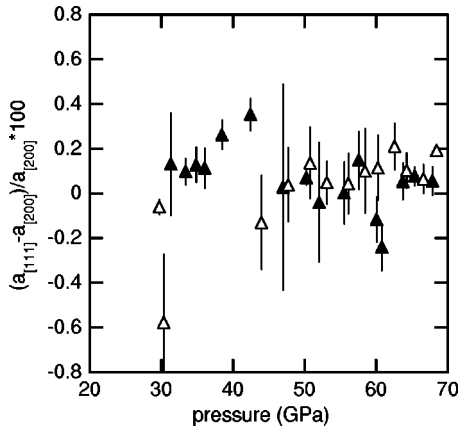

FIG. 3. Normalized difference of the unit-cell parameter a from [200] and [111] peaks of MgO. Open triangle, before annealing; solid triangle, after annealing. Our data scatter was within 0.2%, which is small compared to the nonhydrostatic value of 0.6% (Ref. 13).

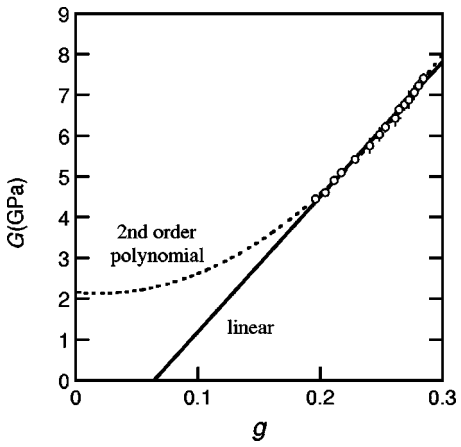

FIG. 4. The g-G relation from Pt calibration data. The curves are fits with a linear function and a second-order polynomial, corresponding to the second- and third-order Birch-Murnaghan EOS, respectively. Use of the linear equation does not provide a good fit to our data. The fit with the second-order polynomial is good but does not cross the $G=0$ axis, which means that it is difficult to constrain the zero-pressure volume with the Birch-Murnaghan EOS.

Figure 6(a) shows our experimental data and the fits with Eqs. (1a) and (3a). Only the Pt calibration data are shown for simplicity. When these results are extrapolated up to 150 GPa, the pressure estimated with the modified universal EOS is about 5 GPa lower than that with the modified third-order Birch-Murnaghan EOS, a difference similar to that between the Pt and MgO calibration data. Therefore, extrapolation to

TABLE II. Fitting parameters with various EOS using the reference volume $V_r = 27.17$ Å^3.

	EOS[a]		
Parameters[b]	Modified second-order BM Eq. (1a)[c]	Modified third-order BM Eq. (1a)	Modified universal Eq. (3a)
	(a) Pt calibration		
P_r (GPa)	30.72 (26)	31.35 (19)	31.14 (14)
K_r (GPa)	158.8 (16)	137.2 (42)	143.5 (6)
K_r'	d	4.85 (35)	
R_P (GPa)	0.49	0.27	0.29
	(b) MgO calibration		
P_r (GPa)	31.78 (18)	32.08 (19)	32.15 (13)
K_r (GPa)	153.8 (11)	143.2 (42)	141.0 (6)
K_r'	d	3.94 (31)	
R_P (GPa)	0.34	0.27	0.27

[a]The numbers in parentheses are uncertainties in the last digit(s).
[b]Defined in the text [see Eqs. (1a), (2), and (3a)].
[c]$K_r' = 4 - 35P_r/9K_r$ in Eq. (1a).
[d]Constrained by $K_r' = 4 - 35P_r/9K_r$.

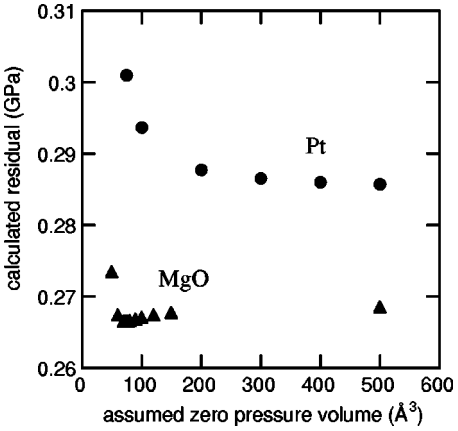

FIG. 5. The fitted residual as a function of zero-pressure volume (V_0) with the universal EOS (Ref. 17). Circle, Pt calibration data; triangle, MgO calibration data. Small residuals can be obtained from a large range of V_0 values. It means that the V_0 is not a critical parameter in characterizing the compression behavior of the NaCl-$B2$ phase.

high pressures is internally consistent for the two equations of state considered here. It should be noted that extrapolation of the current fit to low pressures is inappropriate due to the poor constraint on the zero-pressure volume of the $B2$ phase.

IV. DISCUSSION

Figure 6(b) shows our pressure-volume data compared to the previous experimental observations[2,7] and pseudopotential calculation.[19] The errors of our data are smaller than those from previous experimental studies due presumably to the stress release by the laser annealing treatment in this study. The volume of the $B2$ phase is systematically smaller than in previous experimental studies,[2,7] but in good agreement with the one that was similarly annealed by laser heating[7] [the large open diamond in Fig. 6(b)]. The observed volume discrepancy could be due to the effect of nonhydrostatic conditions. Generally, nonhydrostatic conditions lead to an overestimation of volume by x-ray diffraction with an incident x-ray beam parallel to the DAC loading axis, a diffraction geometry used in this study and the previous experimental studies.[2,7] This effect has been found in other systems, such as $CaSiO_3$ perovskite[15] and MgO.[20] Our data show close agreement with the pseudopotential calculation,[19] although a slight difference in slope exists.

Bassett *et al.*[1] observed the $B1$-$B2$ phase transformation at $V_{B1}=28.83\pm0.07$ Å^3 and $V_{B2}=27.17\pm0.10$ Å^3. From the EOS of the $B1$ phase, the phase transition pressure was estimated to be 30.6 ± 0.5 GPa by Decker,[4] 29.8 ± 0.5 GPa by Birch,[5] and 31.0 ± 0.5 GPa by Brown.[6] The present EOS of the $B2$ phase gives 31.14 ± 0.14 GPa from Pt calibration data and 32.15 ± 0.13 GPa from MgO calibration data with Eq. (3a) and parameters as shown in Table II. By combining all these, the phase transition pressures derived from different EOS lie between 29.3 and 32.3 GPa with an average of 30.8 ± 1.5 GPa. To estimate the difference in volume at the transition, the volume of the $B1$ phase is calculated with the universal EOS (Ref. 17) with parameters of $V_0=44.86$ Å^3,

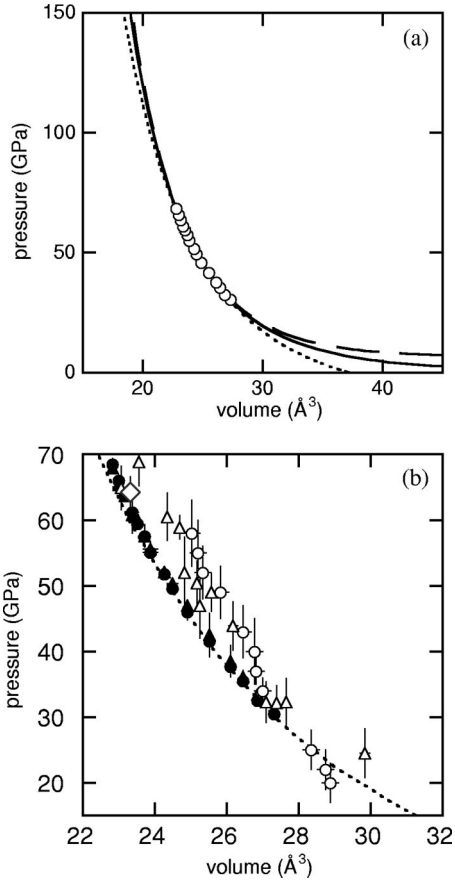

FIG. 6. The volume-pressure relations of the $B2$ phase. (a) The observed data and the fits with parameters as shown in Table II. Only the Pt calibration data are shown for simplicity. Circles, the observed data, the errors are within the symbols; dotted line, the modified second-order Birch-Murnaghan EOS [$K_r'=4-35P_r/9K_r$ in Eq. (1a)] with $P_r=30.72$ GPa and $K_r=158.8$ GPa; dashed line, the modified third-order Birch-Murnaghan EOS [Eq. (1a)] with $P_r=31.35$ GPa, $K_r=137.2$ GPa, and $K_r'=4.85$; solid line, the modified universal EOS [Eq. (3a)] with $P_r=31.14$ GPa and $K_r=143.5$ GPa. (b) Comparison with literature data. Solid circles and triangles, Pt and MgO calibration data in this study; open circles, experimental data (Ref. 2); open triangles and diamond, experimental data (Ref. 7); and dotted line, the pseudopotential calculation (Ref. 19). The annealed datum in a previous experiment (Ref. 7) (a big open diamond at 23.3 Å^3 and 64.3 GPa) is in good agreement with our data.

$K_{01}=23.8$ GPa, and $K_{01}'=5.10$. Here K_{01} and K_{01}' were compiled from compression, ultrasonic, and length-change data.[8] The volume difference ($\Delta V\equiv V_{B2}-V_{B1}$) at 31 GPa is -5.3% by Pt calibration data and -4.6% by MgO calibration data with the modified universal EOS [Eq. (3a)], values slightly smaller than that of Bassett *et al.*[1] (-5.8%).

Using the fitted parameters with the modified universal EOS [Eq. (3)], we calculated the bulk modulus as a function of pressure. It should be pointed out that our bulk modulus data are not directly observed. No explicit errors are included for bulk modulus data. Figure 7(a) shows the calculated pressure and bulk modulus relation compared to IR experimental data,[8] *ab initio* calculation data,[21] and $B1$ phase data.[8,21] All

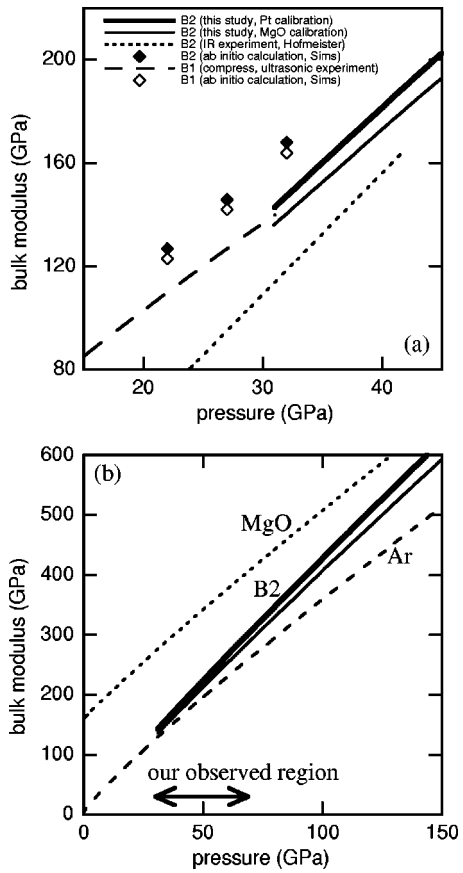

FIG. 7. The pressure-bulk modulus relations of the $B2$ and $B1$ phases. (a) Comparison with the literature data. (b) Comparison with MgO and argon. Thick and thin solid lines are our data of the NaCl-$B2$ phase with Pt calibrant and MgO calibrant. The short dashed line is data of MgO calculated using the Birch-Murnaghan EOS (Ref. 16) with $K_0=160.2$ GPa and $K_0'=3.99$ (Ref. 13). Long dashed line is data of argon calculated using the universal EOS (Ref. 17) with $K_0=3.03$ GPa and $K_0'=7.24$ (Ref. 22). The bulk modulus data show that the $B2$ phase of NaCl is harder than argon, but still softer than MgO.

data show a similar pressure dependence of the bulk modulus (K') for the $B2$ phase, 4.1–4.7 (Table III). Table III shows that the relative bulk modulus difference between the $B1$ and $B2$ phase is consistent with an *ab initio* calculation ($+2\%$), but much different from the IR experiment (-17%). This difference may be due to the second-neighbor effect which was not included in the model used in the IR experiment. This effect has been discussed by Sims *et al.*[21] The absolute values of the bulk modulus in *ab initio* calculations[21] are 20% larger than experimental data for both the $B1$ and $B2$ phases. Since the data for the $B1$ phase from compression, ultrasonic, and IR experiments are consistent

TABLE III. Bulk modulus and related values of the $B2$ phase at 31 GPa.

	This study Pt calibration	This study MgO calibration	IR experiment	*ab initio* calculation
K_{B2} /GPa	143[b]	136[b]	114[d]	164[f]
K'_{B2}	4.3[b]	4.1[b]	4.7[e]	4.4[g]
K_{B1} /GPa	140[c]	140[c]	137[d]	161[f]
ΔK[a]	$+2\%$	-2%	-17%	$+2\%$

[a]Relative bulk modulus difference: $\Delta K\equiv(K_{B2}-K_{B1})/K_{B1}\times 100\%$.
[b]Calculated using Eq. (3b).
[c]Estimated from compiled compression, ultrasonic, and length change data (Ref. 8).
[d]Estimated from IR measurement data (Ref. 8).
[e]Reference 8.
[f]Estimated from *ab initio* data (Ref. 21) using a linear relation.
[g]Reference 21.

with each other, the data of *ab initio* calculations[21] may include systematic errors in absolute values.[21] Shown in Fig. 7(a) and Table III, we conclude that the bulk modulus of the $B2$ phase is similar to the $B1$ phase near the transition pressure, while the pressure dependence of the $B2$ phase is steeper than that of the $B1$ phase.

Figure 7(b) shows the calculated pressure and bulk modulus relation up to 150 GPa compared with other materials commonly used as pressure media in DAC studies.[13,22] The bulk modulus of the $B2$ phase is larger than argon, but smaller than MgO at all pressures up to 150 GPa. Although the shear modulus could be important in selecting materials as a pressure medium, information at high pressures is very limited. The bulk modulus remains a good guidline for selecting a proper medium at high pressure. The bulk modulus data in this study indicate that the $B2$ phase of NaCl is a harder material than the $B1$ phase and argon, but softer than MgO over a pressure range up to 150 GPa.

ACKNOWLEDGMENTS

We thank Emmanuel Soignard, Peter Eng, Takeyuki Uchida, Fred Sopron, Mike Jagger, and Nancy Lazarz for help during the experiment. Thanks are due to Nancy Lazarz for reading this manuscript. N.S. thanks Takehiko Yagi for this research opportunity. This work is supported by NSF-EAR 00011498. Use of the Advanced Photon Source was supported by the U.S. Department of Energy, Office of Science, Office of Basic Energy Sciences, under Contract No. W-31-109-ENG-38. GeoSoilEnviroCARS is supported by NSF-EAR and DOE-Geosciences. This work is supported in part by NFS-EAR 00011498. N.S. is supported by the Japan Society for the Promotion of Science.

*Also at Department of Earth and Planetary Science, University of Tokyo, Tokyo, Japan. Electronic address: sata@cars.uchicago.edu
†Also at Department of Geophysical Sciences, University of Chicago, Chicago, IL 60637.

[1] W. A. Bassett, T. Takahashi, H.-K. Mao, and J. S. Weaver, J. Appl. Phys. **39**, 319 (1968).
[2] Y. Sato-Sorensen, J. Geophys. Res. **88**, 3543 (1983).
[3] X. Li and R. Jeanloz, Phys. Rev. B **36**, 474 (1987).

[4] D. L. Decker, J. Appl. Phys. **42**, 3239 (1971).
[5] F. Birch, J. Geophys. Res. **91**, 4949 (1986).
[6] J. M. Brown, J. Appl. Phys. **86**, 5801 (1999).
[7] D. L. Heinz and R. Jeanloz, Phys. Rev. B **30**, 6045 (1984).
[8] A. M. Hofmeister, Phys. Rev. B **56**, 5835 (1997).
[9] G. Shen, M. L. Rivers, Y. Wang, and S. R. Sutton, Rev. Sci. Instrum. **72**, 1273 (2001).
[10] P. Eng, M. Newville, R. L. Rivers, and S. R. Sutton, Proc. SPIE **3449**, 145 (1998).
[11] A. P. Hammersley, S. O. Svensson, M. Hanfland, A. N. Fitch, and D. Häusermann, High Press. Res. **14**, 235 (1996).
[12] N. C. Holmes, J. A. Moriarty, G. R. Gathers, and W. J. Nellis, J. Appl. Phys. **66**, 2962 (1989).
[13] S. Speziale, C.-S. Zha, T. S. Duffy, R. J. Hemley, and H.-k. Mao, J. Geophys. Res. **106**, 515 (2001).
[14] A. K. Singh, J. Appl. Phys. **73**, 4278 (1993).
[15] S.-H. Shim, T. S. Duffy, and G. Shen, Phys. Earth Planet. Inter. **120**, 327 (2000).
[16] F. Birch, Phys. Rev. **71**, 809 (1947).
[17] P. Vinet, J. H. Rose, J. Ferrante, and J. H. Smith, J. Phys.: Condens. Matter **1**, 1941 (1989).
[18] J.-P. Poirier, *Introduction to the Physics of the Earth's Interior*, 2nd ed. (Cambridge University Press, Cambridge, England, 2000).
[19] S. Froyen and M. L. Cohen, J. Phys. C **19**, 2623 (1986).
[20] Y. Fei, Am. Mineral. **84**, 272 (1999).
[21] C. E. Sims, N. L. Allan, and T. H. K. Barron, Phys. Rev. B **60**, 2968 (1999).
[22] A. P. Jephcoat, Nature (London) **393**, 355 (1998).